

## Electronic Supplementary Materials

For <https://doi.org/10.1631/jzus.A2400068>

# Load-measurement method for floating offshore wind turbines based on a long short-term memory (LSTM) neural network

Yonggang LIN<sup>1</sup>, Xiangheng FENG<sup>1,2,3</sup>, Hongwei LIU<sup>1</sup>, Yong SUN<sup>2,3</sup>

<sup>1</sup>State Key Laboratory of Fluid Power and Mechatronic Systems, Zhejiang University, Hangzhou 310058, China

<sup>2</sup>Windey Energy Technology Group Co., Ltd., Hangzhou 310012, China

<sup>3</sup>Zhejiang Key Laboratory of Wind Power Generation Technology, Hangzhou 310012, China

## Section S1 LSTM equations

$$c(t) = gate_{forget} * c(t-1) + gate_{in} * tanh\left(W_c \begin{bmatrix} x(t) \\ h(t-1) \end{bmatrix} + b_c\right) \quad (S1)$$

$$h(t) = gate_{out} * tanh(c(t)) \quad (S2)$$

$$gate_{forget} = \sigma\left(W_{forget} \begin{bmatrix} x(t) \\ h(t-1) \end{bmatrix} + b_f\right) \quad (S3)$$

$$gate_{in} = \sigma\left(W_{in} \begin{bmatrix} x(t) \\ h(t-1) \end{bmatrix} + b_{in}\right) \quad (S4)$$

$$gate_{out} = \sigma\left(W_{out} \begin{bmatrix} x(t) \\ h(t-1) \end{bmatrix} + b_{out}\right) \quad (S5)$$

where  $W$  and  $b$  represent the weight coefficients and bias coefficients, determined through training with a large amount of data. The  $\sigma$  and  $tanh$  functions are as follows:

$$\sigma(x) = \frac{1}{1 + e^{-x}} \quad (S6)$$

$$tanh = \frac{e^x - e^{-x}}{e^x + e^{-x}} \quad (S7)$$

## Section S2 Geometry model

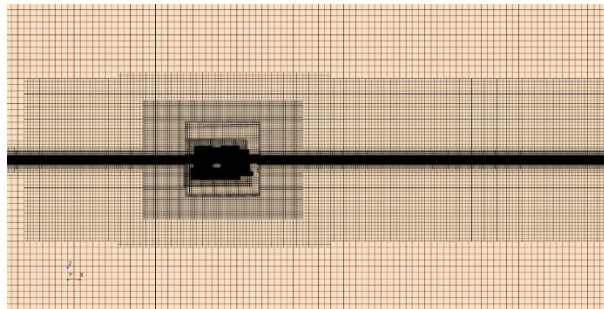
The center column serves as the support structure for the wind turbine. Each column is further divided into upper, middle, and down sections, with the down section designated for accommodating ballast, thereby lowering the system's center of mass and enhancing stability. The geometric dimensions of the platform are detailed in Table S1. The mooring system consists of three catenary lines, which have a length of 700 m and are spaced 120° apart. For more details, one can refer to the previous publication (Feng et al., 2023).

Table S1 Platform geometry dimensions, unit: m.

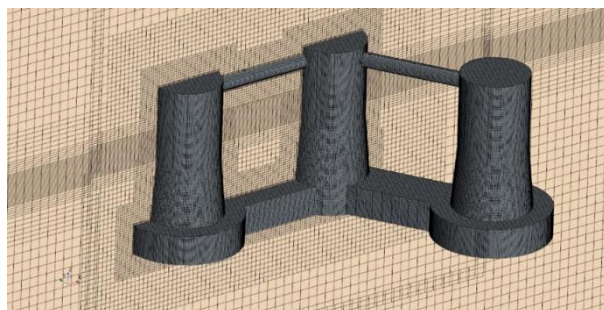
Parameter	Value
Draft	22
Air gap	12
Column height (up, mid, down)	16, 12, 6
Column diameter (up, mid, down)	14, 16, 24
Center distance, a	34.64
Width, d	10
Rod diameter, r	3

### Section S3 Validation of the CFD model

The mesh distribution of the whole fluid domain is depicted in Fig. S1, utilizing an orthogonal grid type. From the far field to the near field, grids were continuously refined to achieve smooth flow field transitions. Besides, refinement grids were created near the free surface and platform surface as well. According to the advice from STAR-CCM+ User Guide, grid sizes near the free surface were set as 2 m, 2 m, 0.125 m in X-Y-Z direction respectively. The grid independence verification results are shown in Table S2. Platform pitch motion RAOs (response amplitude operator) under different numbers of grids were compared. In terms of computational accuracy and cost, 12.7 million grids, with 9.1 million in the background domain and 3.6 million in the motion domain, were adopted for subsequent simulation analysis.



(a)



(b)

Fig. S1 The mesh distribution of the CFD model: (a) mesh in the background domain; (b) mesh on the platform surface.

Table S2 Grid independence verification.

Grids quantity (million)	5.2	9.6	12.7	15.4
Grid size on platform (m)	0.2	0.1	0.05	0.02
Pitch RAO ( $^{\circ}$ /m)	0.107	0.156	0.182	0.189
Relative error (%)	43.38	17.46	3.70	/

The convergence study of time step was completed by carrying out simulations of a fixed platform under a regular wave. The hydrodynamic loads on the platform at four different time steps were recorded in Fig. S2. One can see that the results with the time step of 0.01 s and 0.02 s are close, while the result with the time step of 0.05 s has significant differences. Therefore, the time step of 0.02 s was selected for further analysis.

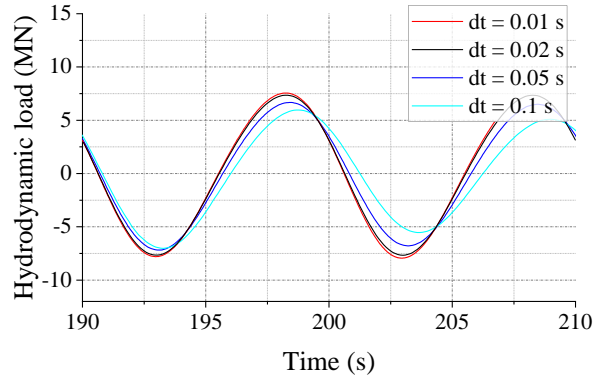


Fig. S2 The convergence of time step.

The accuracy of the CFD model was validated preliminarily through the model test results (Feng et al., 2023). Three characteristic parameters in pitch DOF were compared, as shown in Table S3. Natural period and viscous damping ratio were obtained through the free decay test, and the pitch RAO was obtained through the model test under a regular wave. In general, the CFD model is reliable with each difference of approximately 5%.

Table S3 CFD model validation in pitch DOF.

Parameter	CFD simulation	Experiment	Relative error
Natural period (s)	27.3	28.5	4.21%
Viscous Damping ratio	0.0711	0.0748	4.95%
Pitch RAO ( $^{\circ}$ /m)	0.182	0.193	5.70%

#### Section S4 Statistical parameters in data processing

In this study, the normalized data was used to calculate the average value error  $E_{mean}$ , extreme value error  $E_{max}$ , curve fitting degree  $R_{fit}$  and root mean square error  $RMSE$ , as follows:

$$E\_mean = \frac{|\bar{F}_{cal} - \bar{F}_{true}|}{\bar{F}_{true}} \quad (S8)$$

$$E\_max = \frac{|F_{cal-max} - F_{true-max}|}{F_{true-max}} \quad (S9)$$

$$R\_fit = 1 - \sqrt{\frac{\sum_i^n (F_{cal}^i - F_{true}^i)^2}{\sum_i^n (F_{true}^i)^2}} \quad (S10)$$

$$RMSE = \sqrt{\frac{\sum_i^n (F_{cal}^i - F_{true}^i)^2}{n}} \quad (S11)$$

Among them,  $F_{cal}$  represents the hydrodynamic load calculated by the neural network model,  $F_{true}$  represents the true value,  $\bar{F}_{cal}$  indicates the average value of the calculated load,  $F_{cal-max}$  indicates the maximum value of the calculated load, and  $n$  signifies the length of the load series.

## Section S5 Determination of optimal model

### S5.1 Sample characteristics influence

To evaluate the impact of input characteristics on model accuracy, this study investigated the influence of different input dimensions first. Ideally, the model input should be fed with a total of seven dimensions, including wave elevation, displacement, velocity and acceleration of surge and pitch DOFs. However, it is extremely difficult or expensive to achieve complete motion measurement in the far sea due to the lack of reference objects (Wang et al., 2018). In the current mature measurement system, surge acceleration, pitch velocity and pitch angle can be easily and accurately obtained by the accelerometer and gyroscope. Therefore, this study considered the influence of four inputs (wave height, surge acceleration, pitch angular velocity, pitch angle) on the model accuracy based on actual measurement feasibility. Additionally, the effects of sensor failure during the measurement process were taken into account. Thus, the effects of three inputs (wave height, pitch velocity, pitch angle) and two inputs (wave height, surge acceleration) were also considered in this study. The model calculation results under different input dimensions are shown in the Fig. S3 and Table S4. The seven-input model demonstrates the highest accuracy, with a curve fitting degree of 97.37% and the smallest  $RMSE$  of only 1.43%. Conversely, the three-input model exhibits the poorest accuracy and fails to capture the internal relationship. Comparatively, the two-input model performs better than the three-input model, highlighting the crucial effect of the acceleration input on model accuracy. The four-input model, utilizing easily accessible signals, has a high curve fitting degree (93.67%), making it the selected model for subsequent training.

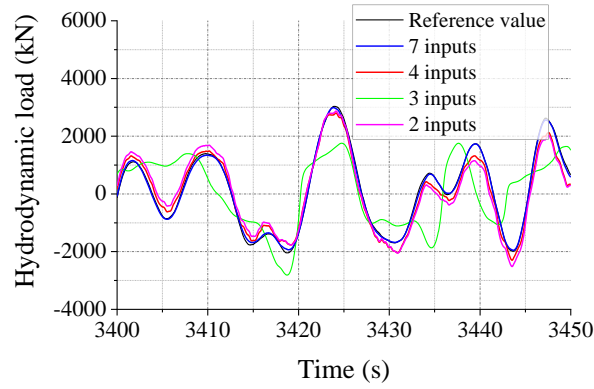


Fig. S3 Influences of input dimensions.

Table S4 Model performances under different input dimensions.

Input dimension	$E_{mean}$	$E_{max}$	$R_{fit}$	$RMSE$
7	1.25%	2.52%	97.37%	1.43%
4	1.74%	1.33%	94.67%	3.44%
3	12.3%	28.63%	68.74%	16.96%
2	2.71%	5.03%	91.95%	4.37%

In addition to the input dimensions, the sampling period of the training data plays a significant role in the model accuracy. A low sampling frequency may overlook the intrinsic features of the training data, while a high sampling frequency will increase training costs and impose hardware requirements. To assess the impact of the sampling period on model accuracy, this study considered four different sampling periods (0.02 s, 0.05 s, 0.1 s, 0.5 s). Models were trained by sample data with four sampling periods, and then tested with sample data with the 0.02 period. Model calculation results and their performances are shown in Fig. S4 and Table S5. The model with a 0.5 s sampling period fails to learn the intrinsic features of the sample data. Conversely, the results with the 0.05 s sampling period demonstrate a good fit effect (94.18%) and low  $RMSE$  (3.16%). Therefore, the sampling period of 0.05 s was adopted for subsequent studies.

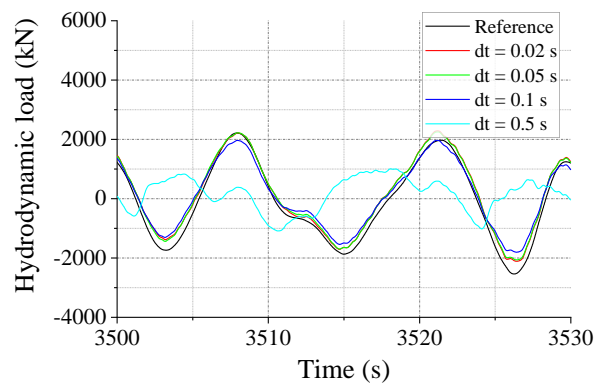


Fig. S4 Influences of sample period.

Table S5 Model performances under different sample periods.

Sampling period (s)	<i>E_mean</i>	<i>E_max</i>	<i>R_fit</i>	<i>RMSE</i>
0.02	1.74%	1.33%	94.67%	3.44%
0.05	2.25%	1.44%	94.18%	3.76%
0.1	3.54%	7.92%	90.58%	5.11%
0.5	27.16%	49.16%	40.15%	32.47%

Sample data is a time series of simulation results, often with a long duration, which need to be divided into several batches for training. To determine an appropriate truncation time length that preserves the inherent mapping characteristics of the sample data and ensures effective training, this study investigated the influence of four different time windows on the training performances. The results are summarized in Table S6. Among these, the time window of 1620 seconds achieves the best prediction effect with the highest curve fitting degree (94.35%) and minimum *RMSE* (3.07%).

Table S6 Model performances under different time windows.

Time window (s)	<i>E_mean</i>	<i>E_max</i>	<i>R_fit</i>	<i>RMSE</i>
405	0.39%	1.76%	93.95%	3.28%
810	1.11%	3.53%	93.89%	3.31%
1620	0.46%	1.07%	94.35%	3.07%
3240	2.25%	1.44%	94.18%	3.76%

## S5.2 Structure parameter influence

Sensitivity analysis of the LSTM layers (1, 2, 3) and neurons (64, 128, 256, 512) were carried out to determine the optimal model structure parameters. Validation results of different model parameters are presented in Table S7 and Table S8. It is evident that the combination of two LSTM layers and 128 neurons in each layer yields the most favorable results. This combination exhibits the highest curve fitting degree, while also having the lowest root mean square error and mean value error. When the number of neurons reaches 512, each error increases rapidly, indicating that the overfitting may have occurred.

Table S7 Model performances under different LSTM layers.

LSTM layers	<i>E_mean</i>	<i>E_max</i>	<i>R_fit</i>	<i>RMSE</i>
1	1.74%	1.33%	93.67%	3.44%
2	0.46%	1.07%	94.35%	3.07%
3	2.18%	1.16%	93.17%	3.71%

Table S8 Model performances under different neuron numbers.

Neuron	<i>E_mean</i>	<i>E_max</i>	<i>R_fit</i>	<i>RMSE</i>
64	0.46%	1.07%	94.35%	3.07%
128	0.047%	1.92%	94.57%	2.95%
256	0.33%	2.10%	94.44%	3.01%
512	7.5%	13.74%	84.29%	8.52%

In addition, training parameters, like solver, learn rate and max epochs, were also considered in this study and adjusted to obtain the best training effect. Finally, the optimal LSTM neural network model was determined after the above sensitivity analysis.

### Section S6 Simulation cases

Wind conditions and wave conditions were shown in Table S9 and Table S10. The wind turbulence was set to Class C, and the irregular sea states were described by the Pierson-Moskowitz spectrum. Finally, the combination of wind and wave conditions totaled 64 cases, as presented in Table S11.

Table S9 Wind conditions.

Wind case	Wind speed (m/s)
I	7.1
II	11.4
III	17.9
IV	44

Table S10 Wave conditions.

Wave case	Significant wave height (m)	Peak period (s)
A	1.67	8.0
B	1.67	8.5
C	1.67	10
D	1.67	16
E	2.5	8.0
F	2.5	8.5
G	2.5	10
H	2.5	16
I	4.29	8.0
J	4.29	8.5
K	4.29	10
L	4.29	16
M	10.9	8.0
N	10.9	8.5
O	10.9	10
P	10.9	16

Table S11 Combined environmental conditions.

Combination case	I	II	III	IV
A	1	2	3	4
B	5	6	7	8
C	9	10	11	12
D	13	14	15	16
E	17	18	19	20
F	21	22	23	24
G	25	26	27	28
H	29	30	31	32
I	33	34	35	36
J	37	38	39	40
K	41	42	43	44
L	45	46	47	48
M	49	50	51	52
N	53	54	55	56
O	57	58	59	60
P	61	62	63	64

### Section S7 Special cases verification

To verify the applicability of the LSTM neural network model in complex environmental conditions, special cases were considered in this study, including wave spectrum, wave direction and current presence, as shown in Table S12. All these cases were created based on previous case 22. The hydrodynamic load calculation results are plotted in Fig. S5 and calculation errors are recorded in Table S13. The LSTM model shows similar calculation performances with previous cases and is still applicable in these complicated sea states. However, it's obvious that the performance of the model is relatively a little bad in different wave direction conditions, with the *RMSE* of 4.84%. Wave directions have significant influences on the hydrodynamic loads. For the future research, one should apply large amount of training cases with small direction angle subdivision to improve the applicability of the LSTM neural network model.

Table S12 Special cases based on case 22.

Verification type	Training cases	Test case
Wave spectrum	Pierson-Moskowitz	Jonswap
Wave direction (°)	0, 10, 20, 40	30
Current velocity (m/s)	0, 0.25, 0.5, 1	0.75

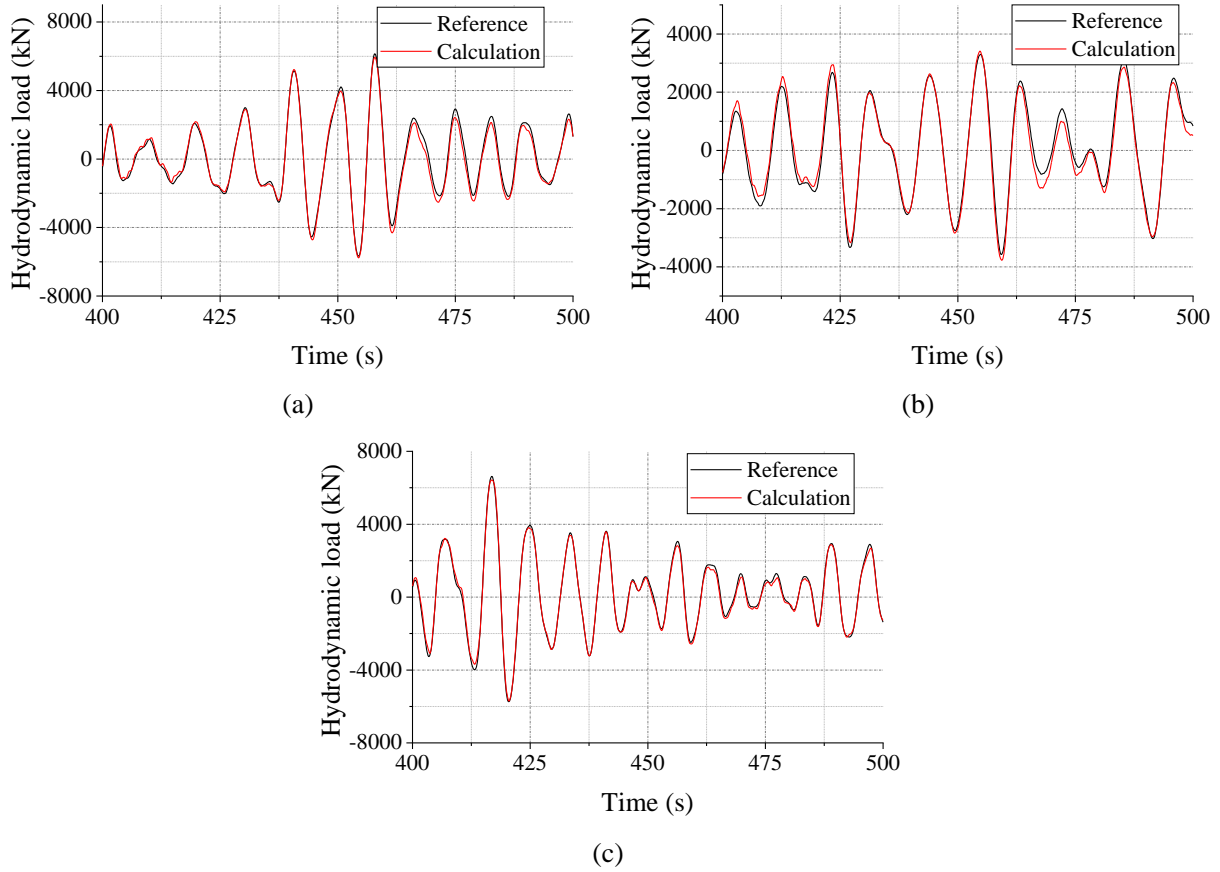


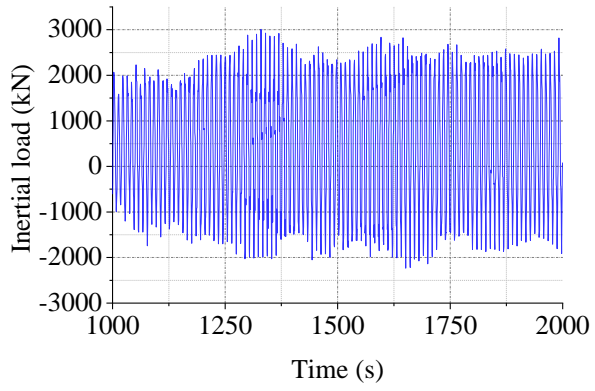
Fig. S5 Model verification under special cases: (a) wave spectrum; (b) wave direction; (c) current presence.

Table S13 Model performances under special cases verification.

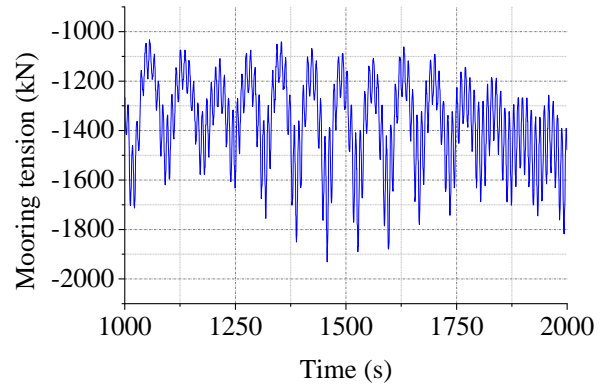
Verification case	$E_{mean}$	$E_{max}$	$R_{fit}$	$RMSE$
Wave spectrum	1.91%	3.01%	94.98%	2.58%
Wave direction	3.86%	4.11%	92.45%	4.84%
Current presence	1.57%	1.44%	96.11%	2.08%

### Section S8 Loads data in Exp1

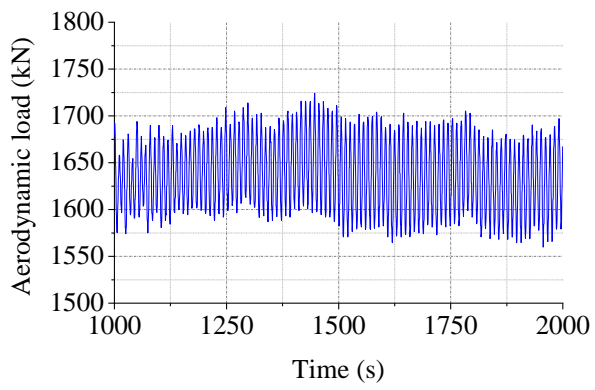
The load history of the FOWT model in Exp 1 was plotted in Fig. S6. The inertial load was calculated by the accelerometer, the constraint load was measured by the mooring tension cell, the aerodynamic load was measured by the tower top load cell. Then, the hydrodynamic load was calculated based on Eq. (S1).



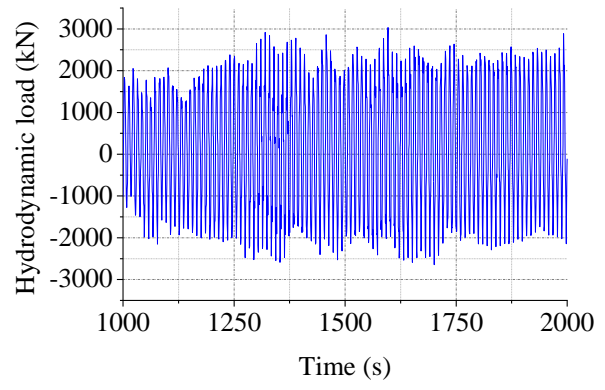
(a)



(b)



(c)



(d)

Fig. S6 Loads data of the FOWT in Exp 1: (a) inertial load  $F_{Inertia}$ ; (b) mooring load  $F_{Mooring}$ ; (c) aerodynamic load  $F_{Aero}$ ; (d) hydrodynamic load  $F_{Hydro}$ .